NACA TN 4313 10655

TECH LIBRARY KAFB, NM
0067208

NATIONAL ADVISORY COMMITTEE FOR AERONAUTICS

TECHNICAL NOTE 4313

EFFECT OF FAVORABLE PRESSURE GRADIENTS ON TRANSITION FOR SEVERAL BODIES OF REVOLUTION AT MACH 3.12

By John R. Jack

Lewis Flight Propulsion Laboratory
Cleveland, Ohio

Washington

July 1958

AFMDC

TECH LIBRARY KAFB, NM
0067208

NATIONAL ADVISORY COMMITTEE FOR AERONAUTICS

TECHNICAL NOTE 4313

EFFECT OF FAVORABLE PRESSURE GRADIENTS ON TRANSITION FOR SEVERAL BODIES OF REVOLUTION AT MACH 3.12

By John R. Jack

4724 CL-1

SUMMARY

Experimental results relating to the effect of pressure gradient on the location of transition are presented for several constant-pressure-gradient models and for two power-profile ($r \propto x^n$) models.

The transition delay increased with increasing favorable pressure gradient. In fact, increasing the constant pressure gradient $[d(p/p_0)/dx]$ from 0 to -0.10 per inch increased the transition Reynolds number to 1.58 times that obtained for the cone model. The distance to transition for both power-profile models was approximately 2.7 times that obtained for the cone. This larger delay in transition has been attributed to the combined effect of blunting and a favorable pressure gradient. In each case, the transition Reynolds number based on local conditions was independent of unit Reynolds number. The data also indicate that local conditions in the tip region are of importance in determining the location of transition.

INTRODUCTION

An investigation of boundary-layer transition with surface cooling (ref. 1) revealed that the transition Reynolds number on a parabolic-nosed body of revolution was approximately double that for a cone-cylinder model. This delay in transition is attributed in reference 1 to the favorable pressure gradient on the parabolic nose. The fact that the transition Reynolds number is increased by a favorable pressure gradient is in agreement with the trends predicted by available stability theories. However, since the pressure gradient was not constant over the nose, the effective magnitude of the pressure gradient causing the delay is unknown. In fact, all the available experimental transition data for bodies of revolution are restricted either to cones that have a zero pressure gradient or to bodies having a varying pressure gradient.

Significant delays in transition have also been obtained by blunting the leading edges of test models (refs. 2 and 3). An exception to this behavior is presented in reference 3, where blunting the parabolic-nosed model failed to increase the transition Reynolds number over that obtained on the sharp parabolic model. This failure to delay transition further by tip blunting was attributed to the region of adverse pressure gradient just downstream of the blunt tip. As a result, it might be anticipated that, if the forebody pressure distribution had been completely favorable, a significant delay in transition would have been obtained.

Therefore, the primary objective of this investigation was to study the combined effects of unit Reynolds number and constant favorable pressure gradients on transition at equilibrium conditions. An additional objective was to determine whether the delay of transition due to tip bluntness could be augmented by a favorable pressure distribution.

4724

SYMBOLS

C_p pressure coefficient, $C_p = \frac{p_l - p_0}{q_0}$

L axial distance to maximum-diameter station

M Mach number

P' nondimensional pressure gradient, $\frac{d\left(\frac{p}{p_0}\right)}{d\left(\frac{x}{L}\right)}$

p static pressure

q dynamic pressure

Re_{tr} transition Reynolds number, $Re = us/\nu$

r body radius

s distance along model surface to location of transition

T absolute temperature

u velocity

u/ν unit Reynolds number

4724

CL-1 back

x	distance along model centerline
γ	ratio of specific heats
δ	local surface inclination
η	recovery factor based on local conditions, $\eta = \frac{T_w - T_l}{T_t - T_l}$
ν	kinematic viscosity

Subscripts:

l	local conditions at edge of boundary layer
max	maximum
N	model vertex
s	at shock
t	stagnation conditions
w	wall values
0	free stream ahead of shock wave

APPARATUS AND PROCEDURE

Wind Tunnel

The models were tested in the NACA Lewis 1- by 1-foot variable Reynolds number tunnel operating at a Mach number of 3.12. Stagnation temperatures were maintained at $80^{\circ} \pm 2^{\circ}$ F, while the stagnation pressure was varied from 7 to 66 pounds per square inch absolute. The resultant unit Reynolds number ranged from 0.83×10^5 to 10×10^5 per inch. All the models were sting-mounted in such a way that the tip of each model was in the same axial location in the tunnel.

Models and Instrumentation

The configurations used for the present investigation are shown in figure 1 along with a sketch showing the pertinent body coordinates. All models were constructed from nickel with a wall thickness of approximately 0.060 inch. The average surface finish for all models as measured by a Brush surface indicator was about 6 microinches. Except for

model 3, every pointed model had a conical tip with an included angle of approximately 18°. Model 3 had a tip included angle of approximately 24°. The tip bluntness of each sharp-nosed configuration was less than 0.005 inch in diameter. According to reference 2, this amount of bluntness should not produce any variation in the distance to transition or in the equilibrium temperature distribution. In addition to the models shown in figure 1, provision was made to attach a cylindrical aft section to model 2. With this provision, the effect of the adverse pressure gradient associated with the cylindrical section could be determined.

Surface temperatures were obtained by measuring the electrical outputs of copper-constantan thermocouples installed on the top generator of each model at 1/2-inch intervals. The millivolt outputs were read automatically with a digital potentiometer and recorded on punch tape. The surface temperatures obtained in this manner are believed to be accurate to ±0.5° F. Model and tunnel wall static-pressure distributions were measured on butylphthalate differential manometers to an accuracy of ±0.002 pound per square inch. Stagnation pressures were accurate to approximately ±0.05 pound per square inch.

4724

Model Design Procedure for Constant Pressure Gradient

It was desired to design a sharp-tipped body contour having a linear pressure distribution (or a constant pressure gradient). Such a contour could be calculated by the method of characteristics (ref. 4); however, this approach is very time-consuming. As a result, an approximate method was derived based on the theory of reference 5.

If it is assumed that the body is slender (i.e., the body slopes are small) and the Mach number is large, the local Mach number is given by

$$M = \frac{M_N}{1 - \frac{\gamma - 1}{2} M_N \delta_N \left(1 - \frac{\delta}{\delta_N}\right)} \tag{1}$$

where M_N is the surface Mach number at the vertex of the model, and δ_N is the flow inclination at the vertex of the model or the cone half-angle. Solving equation (1) for the local surface inclination δ yields

$$\delta = \delta_N - \frac{2}{\gamma - 1}\left(\frac{1}{M_N} - \frac{1}{M}\right) = \tan^{-1} \frac{dr}{dx} \tag{2}$$

To the order of accuracy of the analysis reported in reference 5, the ratio of the local surface Mach number to that at the shock can be expressed in the form

4724

$$\frac{M}{M_s} = \left(\frac{p_s/p_0}{p/p_0}\right)^{\frac{\gamma-1}{2\gamma}} \tag{3}$$

where p_s and M_s are the static pressure and Mach number, respectively at the shock. The pressure rise at the shock (p_s/p_0) is given by

$$\frac{p_s}{p_0} = 1 + \gamma\,(M_0\delta_N)^2 \tag{4}$$

while the Mach number ratio is given by

$$\frac{M_s}{M_0} = \left\{\frac{1 + \frac{\gamma+1}{2}(M_0\delta_N)^2}{\left(\frac{p_s}{p_0}\right)\left[1 + \frac{\gamma-1}{2}(M_0\delta_N)^2\right]}\right\}^{1/2} \tag{5}$$

Equation (2), in terms of known quantities and the static-pressure distribution, finally reduces to

$$\delta = \tan^{-1}\frac{dr}{dx} = \delta_N - \frac{2}{\gamma-1}\left[\frac{1}{M_N} - \frac{\left(\frac{p}{p_0}\right)^{\frac{\gamma-1}{2\gamma}}}{\left(\frac{p_s}{p_0}\right)^{\frac{\gamma-1}{2\gamma}}\,M_s}\right] \tag{6}$$

If a linear pressure distribution is assumed and δ is considered small $(\tan\delta = \delta)$, equation (6) becomes

$$\frac{dr}{dx} = A + B(ax + b)^{\frac{\gamma-1}{2\gamma}} \tag{7}$$

where

$$A = \delta_N - \frac{2}{\gamma-1}\frac{1}{M_N}$$

$$B = \frac{2}{\gamma - 1}\left[\frac{1}{\left(\frac{p_s}{p_0}\right)^{\frac{\gamma-1}{2\gamma}} M_s}\right] = \frac{2}{\gamma - 1}\left[\frac{1}{\left(\frac{p_N}{p_0}\right)^{\frac{\gamma-1}{2\gamma}} M_N}\right]$$

$$a = \frac{d(p/p_0)}{dx}$$

$$b = \frac{p_N}{p_0}$$

Equation (7) may now be integrated to give the body contour having a linear pressure distribution. The contour is given by

$$r = Ax + B\left[\frac{2\gamma}{a(3\gamma - 1)}(ax + b)^{\frac{3\gamma-1}{2\gamma}}\right] + C \qquad (8)$$

The integration constant is determined from the tip conditions ($x = 0$, $r = 0$). The equation describing the desired contour finally becomes

$$r = Ax + \frac{2\gamma B}{(3\gamma - 1)a}\left[(ax + b)^{\frac{3\gamma-1}{2\gamma}} - (b)^{\frac{3\gamma-1}{2\gamma}}\right] \qquad (9)$$

As a check for equation (9), the example calculated by the characteristics method of reference 4 was also calculated using equation (9). A comparison of the two calculations shows that the maximum difference between the two radii was approximately 6 percent. Hence, it is anticipated that equation (9) will yield a body contour having a reasonably linear pressure distribution.

RESULTS AND DISCUSSION

Local Flow Conditions

Typical pressure and Mach number distributions for all models but the cone are presented in figures 2 and 3, respectively. As indicated in the figures, both the pressure and Mach number distributions are fairly linear for models 2 and 3. A comparison of the experimental pressure data with the design pressure distribution shows that the pressure gradient of the experimental data is less negative than the design

gradient. The difference noted in the pressure gradient is attributed to the hypersonic approximations in the design method and the accuracy to which the body was made. It is of special interest for the power-profile models ($r \propto x^n$, models 4 and 5) to note that, aside from the small adverse pressure gradient existing on the cylindrical section, the pressure distribution appears to be completely favorable.

4724

Recovery-Factor Distributions

Typical recovery factors η, based on local flow conditions, are presented in figure 4 for each model at a unit Reynolds number of 6.25×10^5 per inch. For convenience, the distance to the location of transition was measured along the model centerline, except for the power-profile models 4 and 5, where distance along the surface was used. The location of transition was chosen at the station where the recovery factor or the equilibrium temperature first reached a maximum value. The transition point defined in this manner is usually in good agreement with the location picked from schlieren pictures if the model pressure gradient is zero (fig. 4(a)). However, there are nonzero-pressure-gradient cases (figs. 4(d), (e), and (f)) where the peak recovery method and the schlieren location do not agree.

A comparison of figures 4(d), (e), and (f) shows that, as the nose pressure gradient becomes large negatively, the schlieren indication of transition moves upstream from the peak recovery factor towards the initial rise in recovery factor. With with outlook, the peak recovery factor would be more closely associated with the end of transition than the beginning. In addition to this complication, reference 6 has reported that the indication of transition from hot-wire traces is appreciably ahead of the station that would be obtained from schlieren pictures. In fact, the schlieren photographs indicated the location of transition to be an average of 25 percent farther downstream than that identified from the hot-wire traces.

To further complicate matters, the recovery-factor distribution could be significantly affected by wall conduction. The effect of wall conduction on cone recovery-factor distributions is reported in reference 7, which shows that, as the wall thermal conductivity increased, the location of the initial rise in recovery factor moved upstream of the location obtained for a wall with a very low conductivity and the peak value moved downstream. Consequently, the actual transition location must lie someplace between the initial rise in recovery factor and the peak.

The net result of the preceding discussion is that some doubt has been cast upon the use of recovery-factor distributions to establish the absolute location of transition. However, the use of peak recovery factors should provide the relative effects of pressure gradients.

Effect of Unit Reynolds Number

The results of the investigation are summarized in figure 5, where the distance to transition is plotted as a function of local unit Reynolds number. In general, the slope of these curves is -1, indicating that the transition Reynolds number (based on local conditions) is a constant for each constant-pressure-gradient model over a unit Reynolds number range extending from approximately 2×10^5 to 10×10^5 per inch.

Also included in figure 5 for comparison is the faired curve for a 10°-included-angle cone which was tested in the same wind tunnel (ref. 2). A comparison of this curve with the curve obtained from the 18°-included-angle cone used in the present investigation (model 1) shows different slopes. In fact, the transition Reynolds number based on local conditions for the 10° cone was not a constant, but was given by $Re_{tr} = 45{,}900\left(\frac{u_l}{\nu_l}\right)^{0.34}$. At first this behavior is surprising; however, if the basic difference between the two models (local conditions) is considered, a possible explanation of this behavior may be found. The 10° cone has a local Mach number of 3.0, whereas the 18° cone has a local Mach number of 2.8. Now, an examination of the transition results for a 10° cone presented in reference 8 shows that, as the local Mach number decreases, the slope of the curve of transition distance against unit Reynolds number becomes more negative. Therefore, the fact that two different slopes were found for two different cone angles is consistent with other results. However, the preceding discussion does make the effect of local Mach number on the transition Reynolds number discussed in references 2 and 7 uncertain. This effect is illustrated in the following sketch:

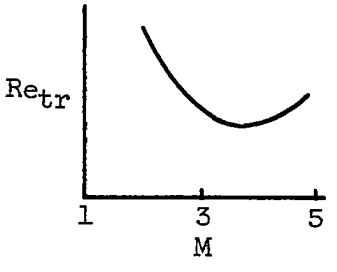

(a)

The unit Reynolds number at which these data were obtained for this effect was about 3×10^5 per inch. Now, based on the data presented herein for the two cones (see sketch (b)), it appears that, if the unit Reynolds

4724

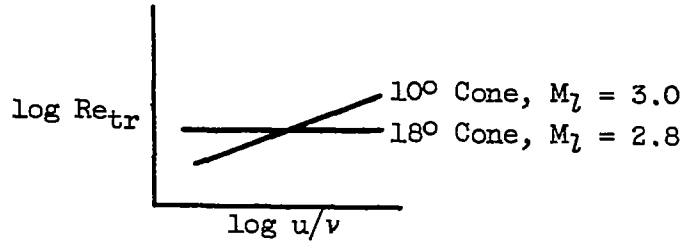

(b)

number u/ν is high enough, the trend of the curve shown in sketch (a) could be completely reversed, or the low point of the curve could be shifted to a Mach number considerably less than that presented in reference 7. These arguments are certainly not conclusive, but it appears that the effect of local Mach number on the transition Reynolds number has not been completely defined and may be substantially changed by the unit Reynolds number.

Effect of Pressure Gradient

The effect of favorable pressure gradients is illustrated in figure 6, where the ratio of local transition Reynolds number with pressure gradient to that without (model 1) is plotted against the experimental pressure gradient. For the constant-pressure-gradient bodies this Reynolds number ratio increases with the nondimensional pressure gradient, $P' = d(p/p_0)/d(x/L)$, to a value of 1.58 for model 3.

The length L used to make the pressure gradient P' nondimensional is the axial distance to the maximum-diameter station. This length is not arbitrary but is defined by the pressure distribution and may be obtained from equation (7). This yields

$$L = \frac{-b + \left(-\frac{A}{B}\right)^{\frac{2\gamma}{\gamma-1}}}{a}$$

However, it should be noted that, although L makes the pressure gradient nondimensional, it does not make it independent of scale. This may be shown as follows:

$$\frac{d\left(\frac{p}{p_0}\right)}{d\left(\frac{x}{L}\right)} = La = -b + \left(\frac{-A}{B}\right)^{\frac{2\gamma}{\gamma-1}} = f(\delta_N)$$

As a result, the experimental data do reflect the effect of cone angle δ_N on the location of transition.

Figure 6 also indicates that, in order to get any sizable increase in the transition Reynolds number by means of a favorable pressure gradient, P' must be in the neighborhood of -1.0. In addition, an approximate value for the sharp parabolic-nosed model of reference 1 is included in figure 6. Using a local Reynolds number ratio of 1.7, which is approximately the equilibrium value, and evaluating the pressure gradient at the leading edge, the point falls in line with the curve presented in figure 6. Thus, it appears that the local conditions in the tip region may be very significant in determining the location of transition.

4724

The effect of a small adverse pressure gradient preceded by a favorable gradient (model 2 and cylindrical section) may be seen by referring to figure 5. For some time, it was thought that perhaps this condition would adversely influence the location of transition. Although only two points were obtained on the cylindrical section, the results indicate that, for the conditions of the investigation, the small adverse pressure gradient existing on the cylindrical section of the model does not influence the location of transition appreciably. In fact, it might be concluded that the conditions on the forebody control the location of transition.

Since both power-profile models have favorable pressure distributions on the nose section (see figs. 2(d) and (e)), it was expected that the blunting effect discussed in reference 8 would be augmented by the favorable pressure gradients. (Based on the previous discussion, it is believed that the effect of the adverse pressure gradient on the cylindrical section was negligible.) The data obtained for both the cone and the power-profile models are presented in figure 7 in terms of the free-stream unit Reynolds number. This type of presentation is used because it best illustrates the actual physical delay in the location of transition. The expectation was fulfilled, for the distance to transition was increased by a factor of about 2.7 times that obtained for a sharp cone (see fig. 7) and approximately twice the maximum value (1.3) obtained for a hemispherically blunted cone (see ref. 2). To the author's knowledge, this is the largest transition delay reported to date under equilibrium conditions for an axially symmetric body at $M \approx 3$.

The set of data obtained for the power-profile models also supports the conclusion that the local conditions in the tip region are controlling the location of transition. This may be seen readily from figure 8, where the forebody pressure distribution for both power-profile models is compared with that for model 2. It is to be noted that the pressure gradients in the tip region are quite large, whereas those downstream of this region are very close to zero.

Reference 2 has reported that the maximum experimental transition delay obtained on a hemispherically blunted cone was 1.3, whereas the theoretical value predicted by reference 9 for a zero-pressure-gradient model is 2.17. The failure to achieve the theoretical delay was partially attributed to the adverse pressure gradient associated with the tip region. On the other hand, the blunt power-profile models, which had completely favorably pressure distributions on their nose sections, gave a transition delay of approximately 2.7. Therefore, it appears that the transition delay due to blunting predicted in reference 9 for axisymmetric bodies is not obtained in the absence of a completely favorable nose pressure distribution. When the effects of blunting and favorable pressure distributions are combined, however, the predictions of reference 9 may be fulfilled or may be exceeded considerably.

SUMMARY OF RESULTS

A study of the equilibrium temperature distributions for three models having varying degrees of constant pressure gradients and for two power-profile models has given the following results:

1. The ratio of local transition Reynolds number with constant pressure gradient to that with zero gradient increases with increasing favorable pressure gradient. The largest value of the Reynolds number ratio was 1.58, and this was obtained with the model having a constant pressure gradient $\left[d(p/p_0)/dx\right]$ of -0.10 per inch.

2. The transition Reynolds number ratio (based on free-stream conditions) obtained for both power-profile models was approximately 2.7. This large delay in transition has been attributed to the blunting effect augmented by a favorable pressure distribution.

3. Contrary to previously reported results for cones and cylinders, the transition Reynolds number based on local conditions for each of the constant-pressure-gradient models was independent of unit Reynolds number.

4. A comparison of the transition location defined by the peak recovery factor with that obtained from schlieren pictures shows that, as the nose pressure gradient becomes large negatively, the schlieren indication of transition moves upstream towards the initial rise in recovery factor. As a result, doubt has been cast upon the use of recovery-factor distributions to establish the absolute location of transition.

Lewis Flight Propulsion Laboratory
National Advisory Committee for Aeronautics
Cleveland, Ohio, April 25, 1958

REFERENCES

1. Jack, John R., and Diaconis, N. S.: Variation of Boundary-Layer Transition with Heat Transfer on Two Bodies of Revolution at a Mach Number of 3.12. NACA TN 3562, 1955.

2. Brinich, Paul F., and Sands, Norman: Effect of Bluntness on Transition for a Cone and a Hollow Cylinder at Mach 3.1. NACA TN 3979, 1957.

3. Diaconis, N. S., Jack, John R., and Wisniewski, Richard J.: Boundary-Layer Transition at Mach 3.12 as Affected by Cooling and Nose Blunting. NACA TN 3928, 1957.

4. Burbank, Paige B.: A Method for Calculating the Contour of Bodies of Revolution with a Prescribed Pressure Gradient at Supersonic Speed with Experimental Verification. NACA TN 3555, 1956.

5. Eggers, A. J., Jr., and Savin, Raymond C.: Approximate Methods for Calculating the Flow About Nonlifting Bodies of Revolution at High Supersonic Airspeeds. NACA TN 2579, 1951.

6. Potter, J. Leith, and Whitfield, Jack D.: Preliminary Study of the Effect of Unit Reynolds Number on Transition Sensitive Data. TN 57-37, Arnold Eng. Dev. Center, 1957. (Contract AF 40(600)-700.)

7. Laufer, John, and Marte, Jack E.: Results and a Critical Discussion of Transition-Reynolds-Number Measurements on Insulated Cones and Flat Plates in Supersonic Wind Tunnels. Rep. No. 20-96, Jet Prop. Lab., C.I.T., Nov. 30, 1955. (Contract DA-04-495-Ord 18, Dept. Army, Ord. Corps.)

8. van Driest, E. R., and Boison, J. Christopher: Research on Stability and Transition of the Laminar Boundary Layer - Covering Experiments on a 20-Inch 10 Degree (Apex Angle) Cone in the 12-Inch Supersonic Wind Tunnel of the Jet Propulsion Laboratory. Rep. No. AL-2196, North Am. Aviation, Inc., Sept. 1, 1955.

9. Moeckel, W. E.: Some Effects of Bluntness on Boundary-Layer Transition and Heat Transfer at Supersonic Speeds. NACA Rep. 1312, 1957. (Supersedes NACA TN 3653.)

4724

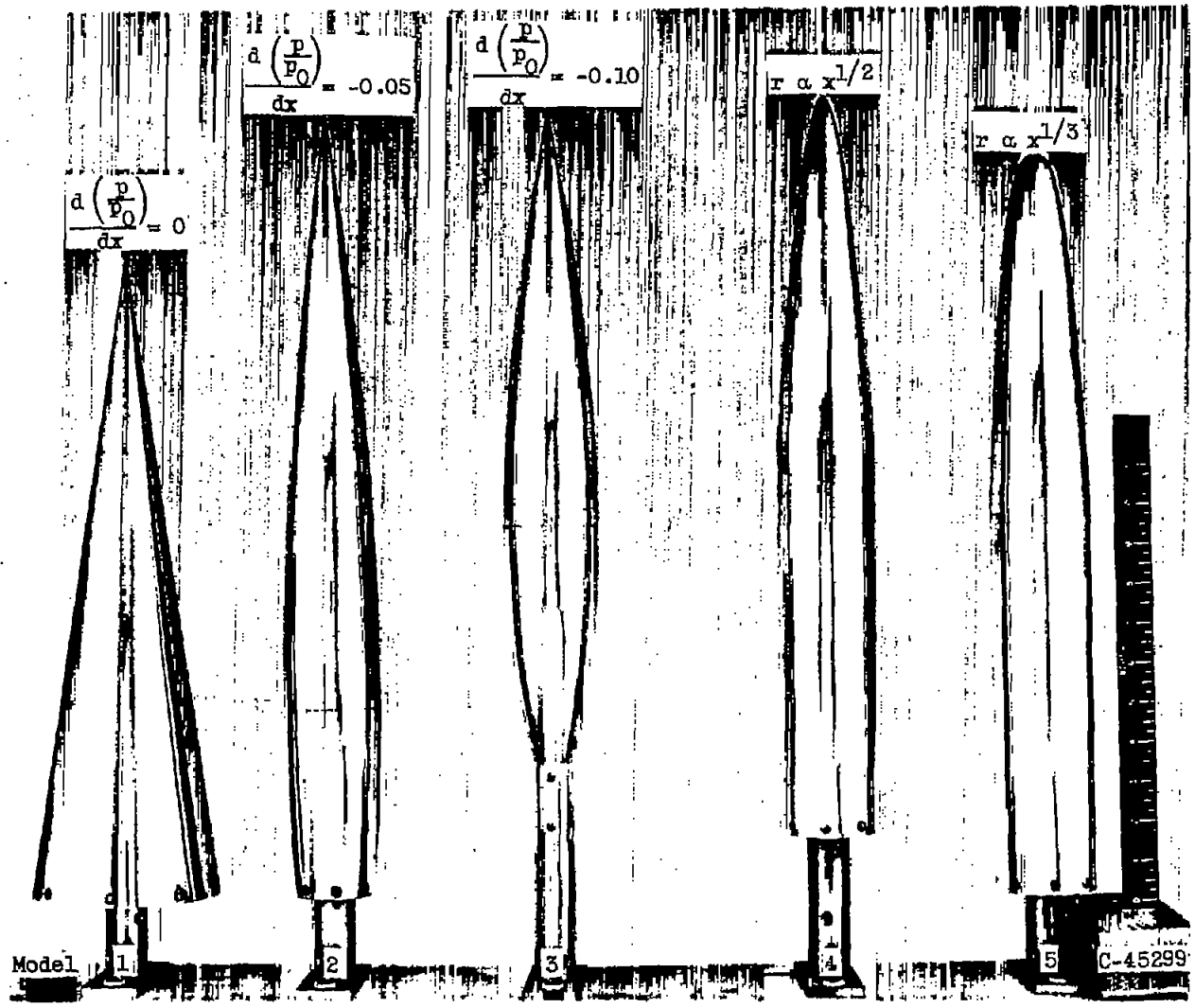

(a) Photographs of models.

Figure 1. - Model configurations investigated.

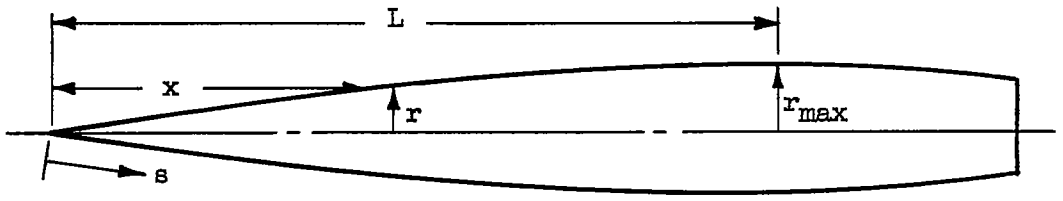

Model	$\frac{d(p/p_0)}{dx}, \frac{1}{in.}$	L, in.	r_{max}, in.
1	0	16.56	2.50
2	-.05	14.90	1.30
3	-.10	10.60	1.26

Constant-pressure-gradient models

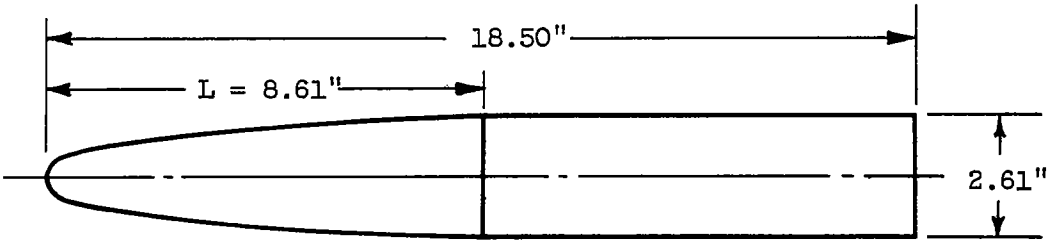

Model	
4	$r_{max}\left(\frac{x}{L}\right)^{1/2}$
5	$r_{max}\left(\frac{x}{L}\right)^{1/3}$

Power-profile models

(b) Model Dimensions.

Figure 1. - Concluded. Model configurations investigated.

4724

4724

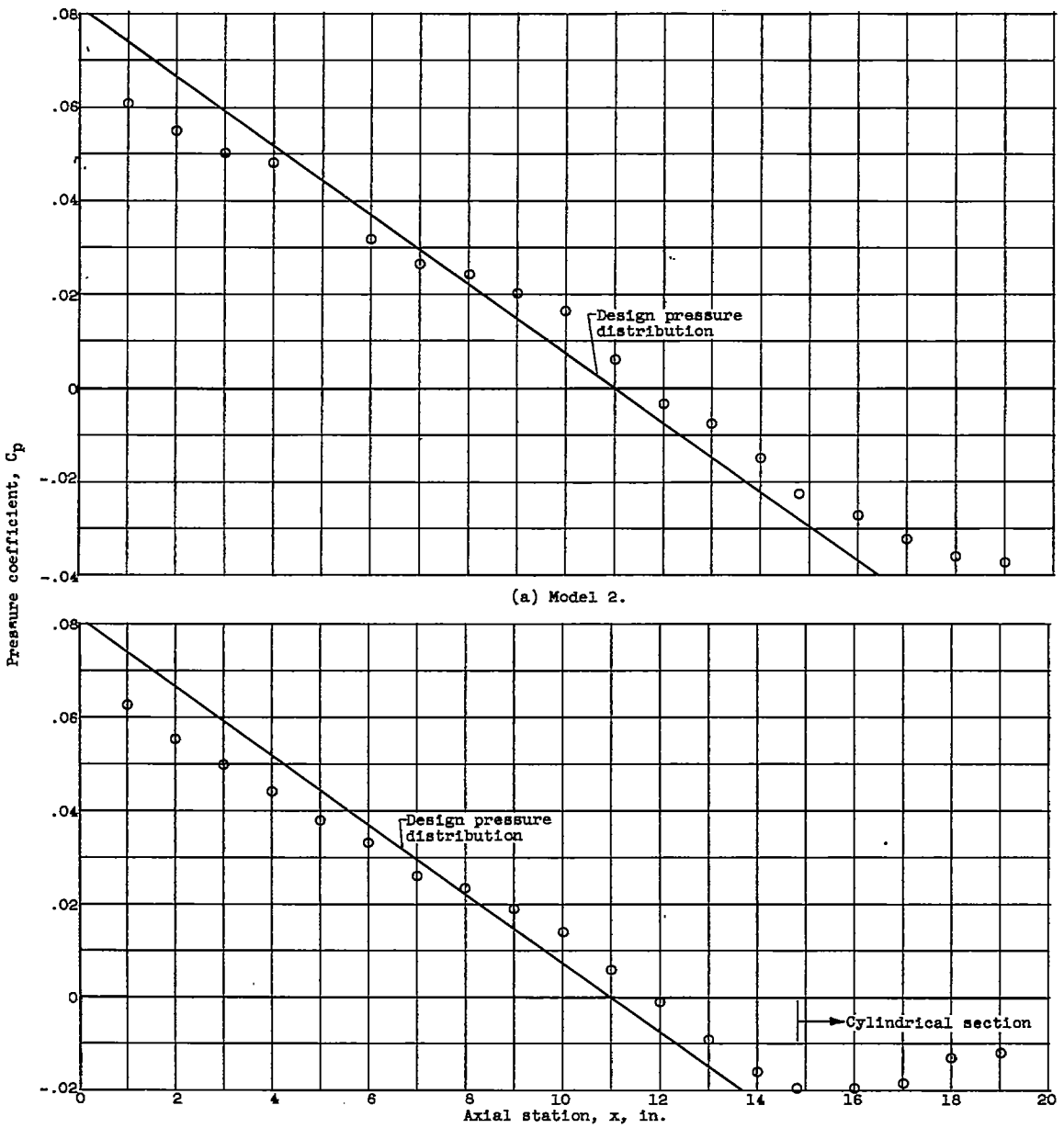

(b) Model 2 plus cylindrical section.

Figure 2. - Surface pressure distribution.

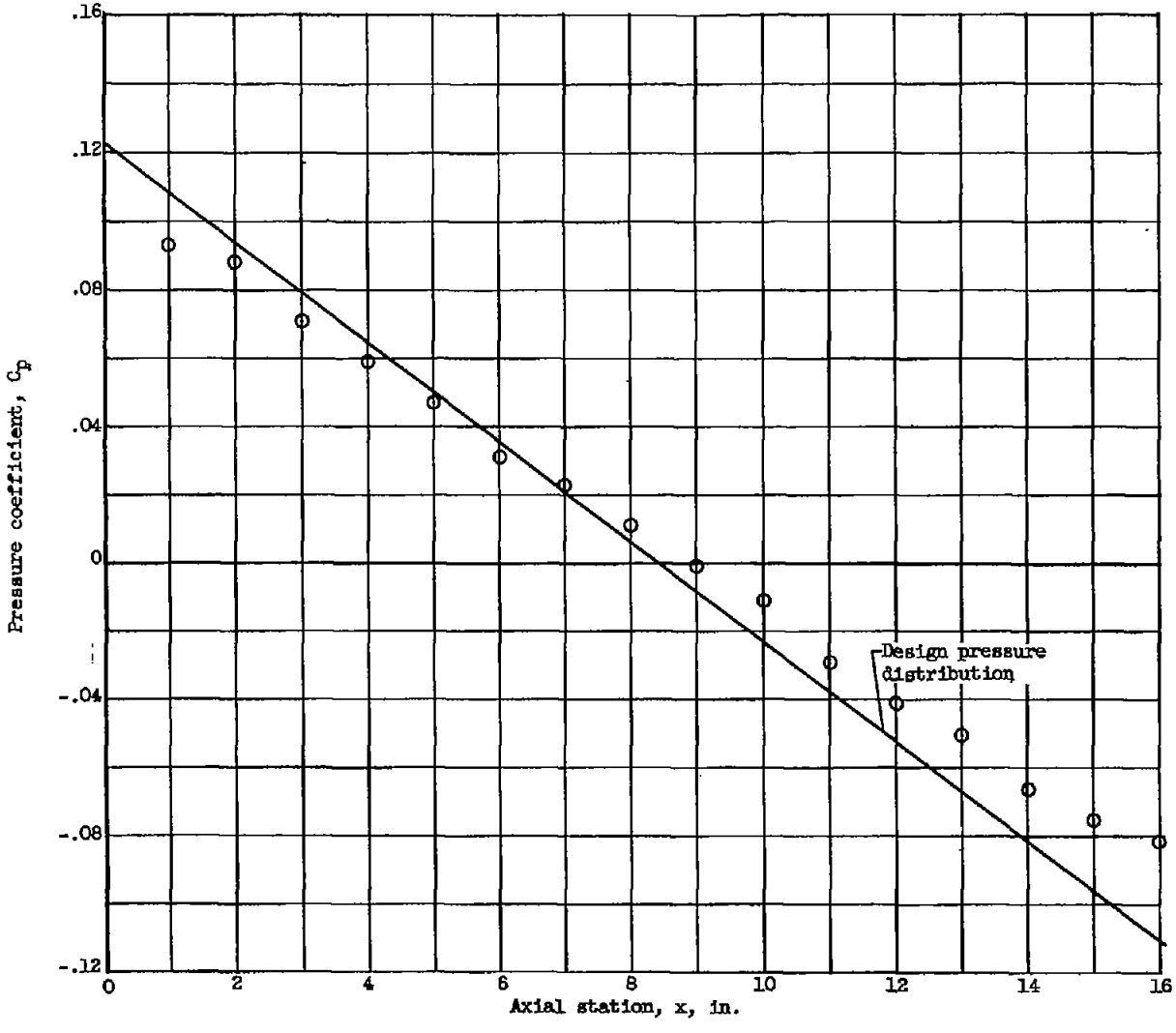

(c) Model 3.

Figure 2. - Continued. Surface pressure distribution.

4724 CL-3

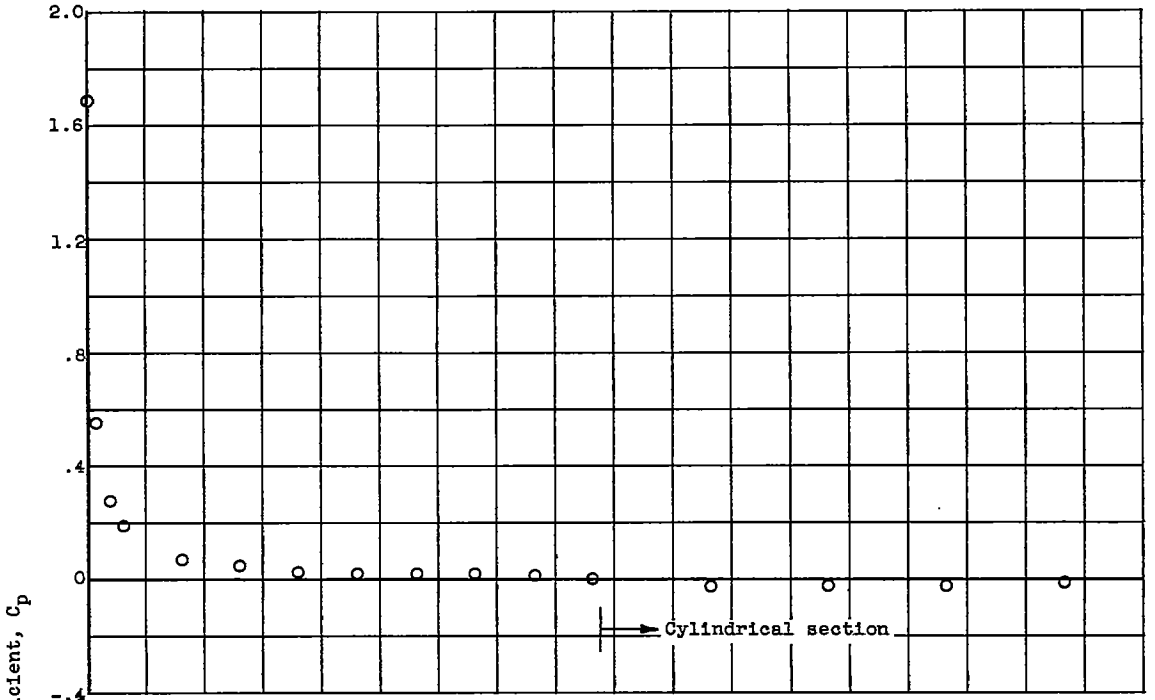

(d) Model 4.

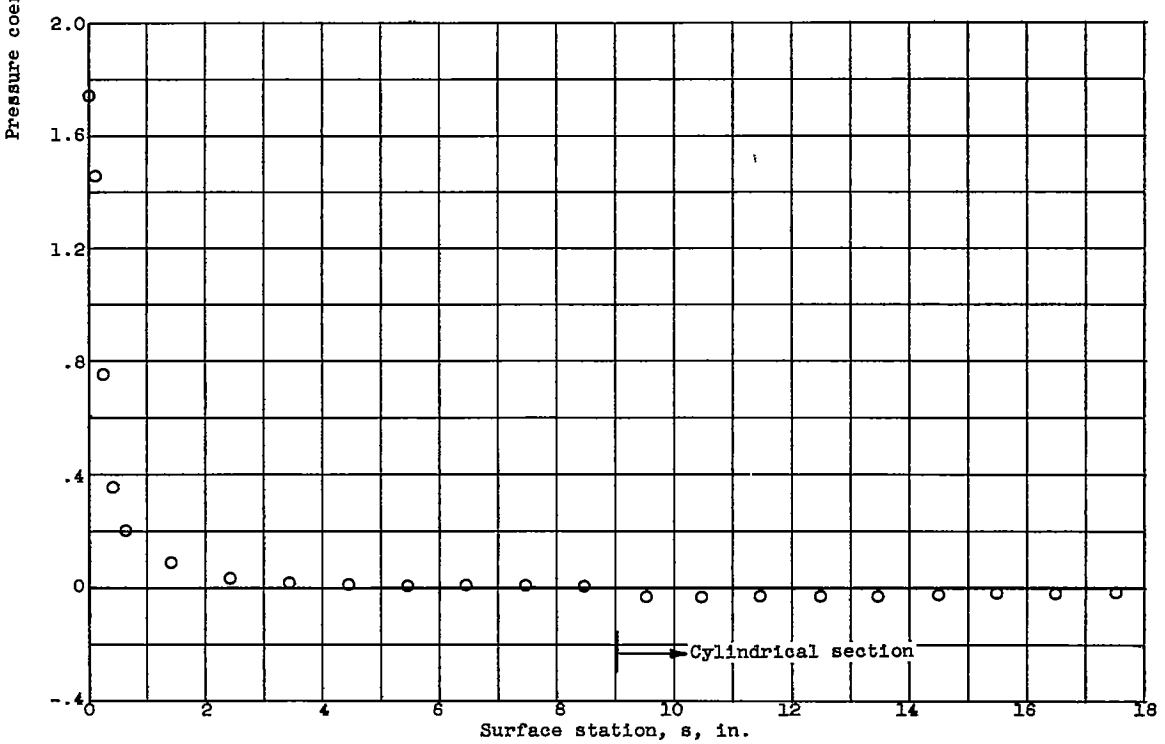

(e) Model 5.

Figure 2. - Concluded. Surface pressure distribution.

4724

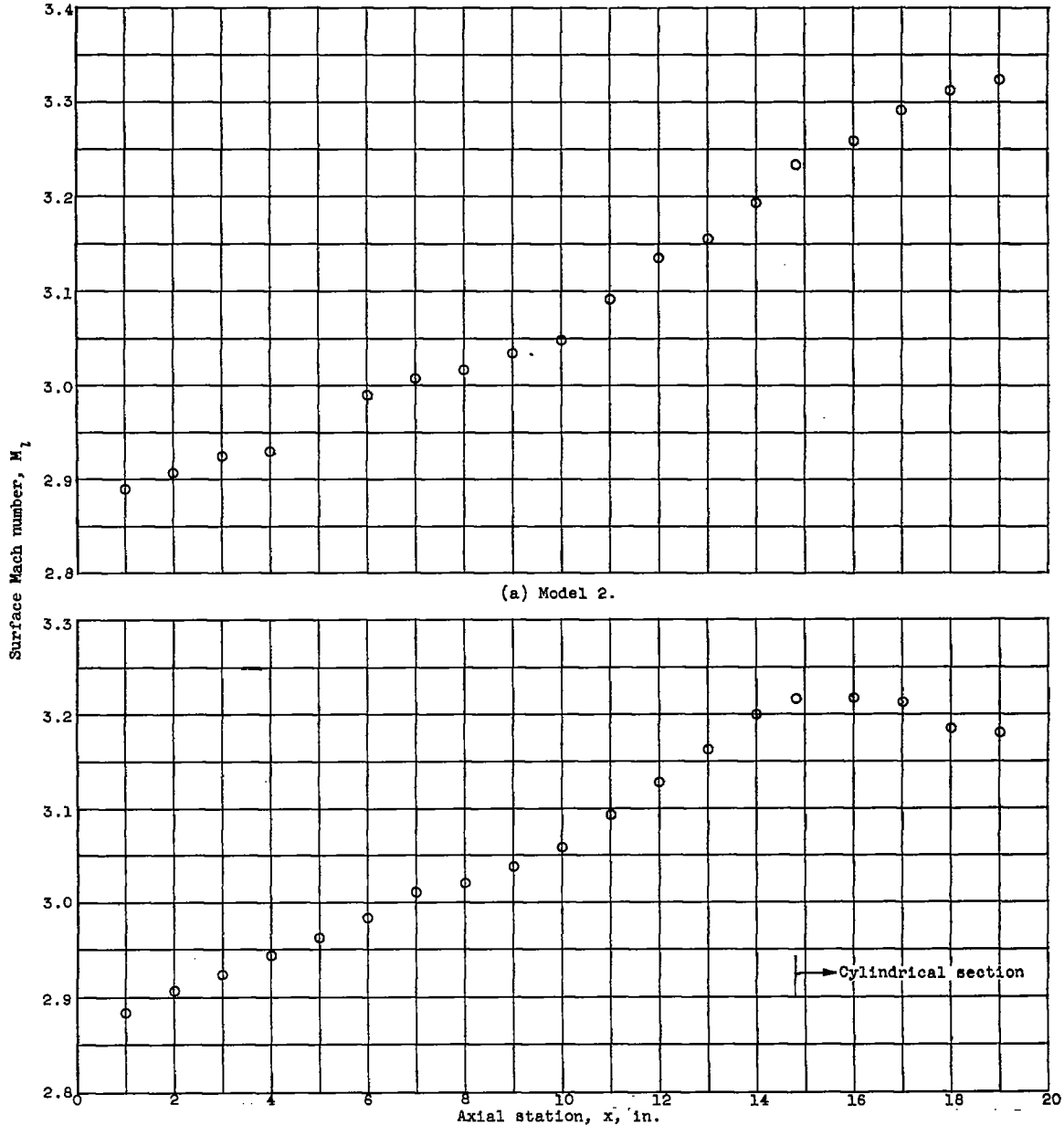

(a) Model 2.

(b) Model 2 plus cylindrical section.

Figure 3. - Surface Mach number distribution.

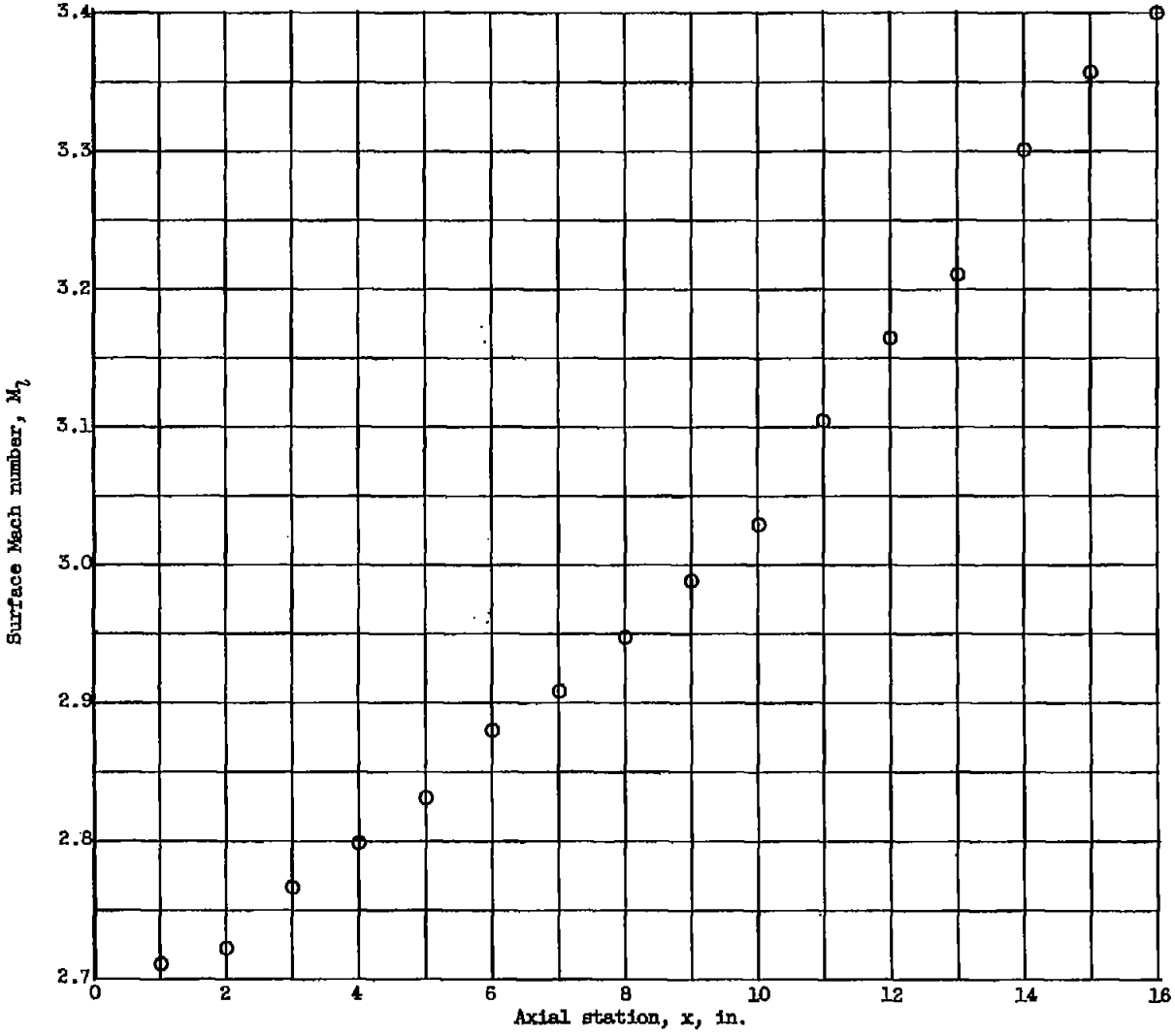

(c) Model 3.

Figure 3. - Continued. Surface Mach number distribution.

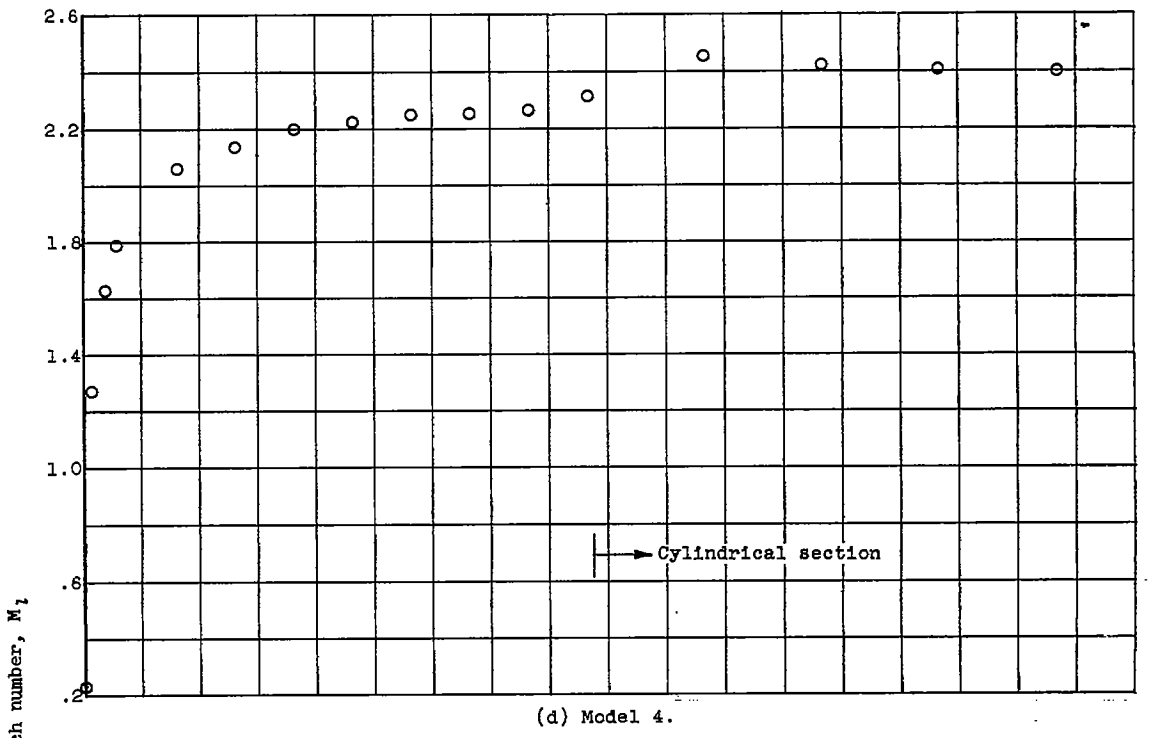

(d) Model 4.

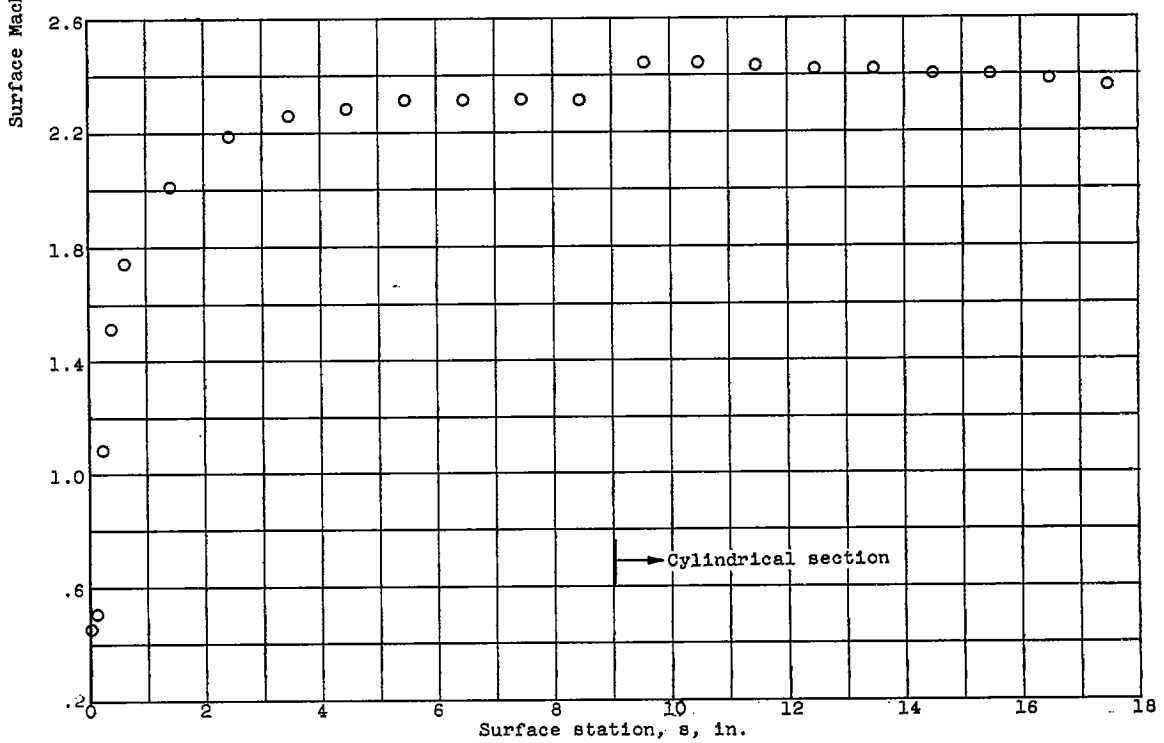

(e) Model 5.

Figure 3. - Concluded. Surface Mach number distribution.

4724

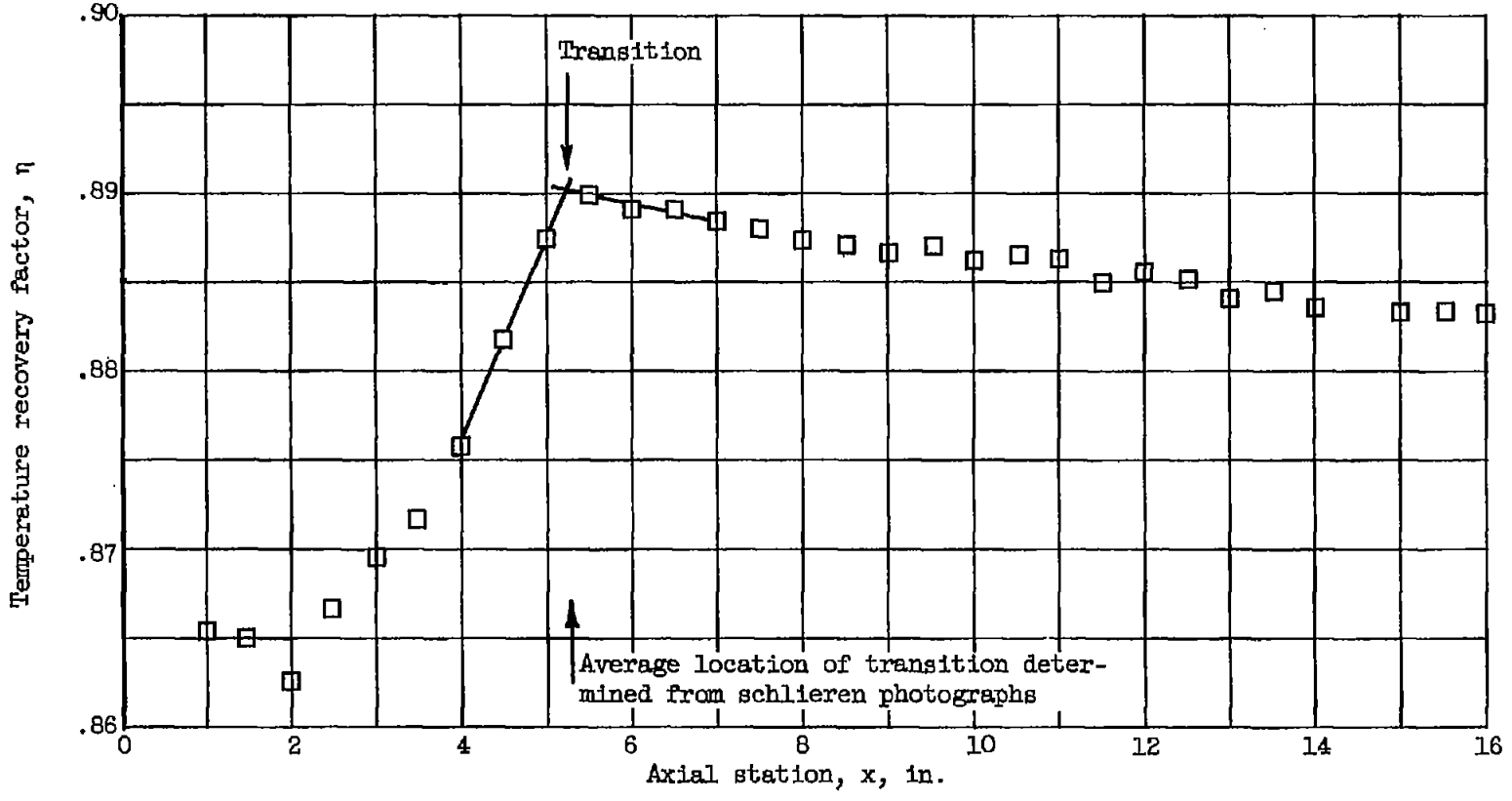

(a) Model 1.

Figure 4. - Typical temperature-recovery-factor distribution. Free-stream unit Reynolds number, u_0/ν_0, 6.25×10^5 per inch.

4724

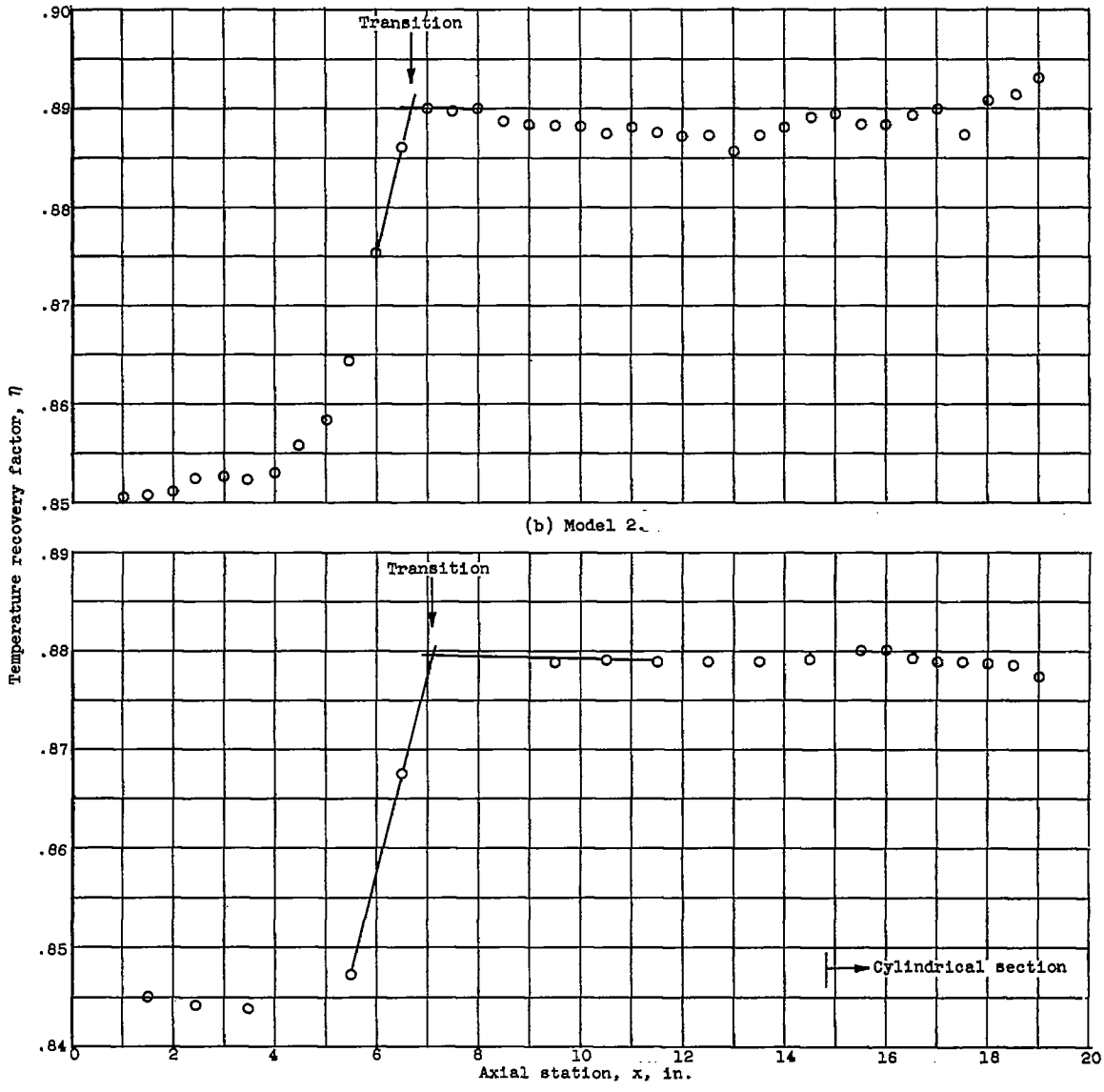

(c) Model 2 plus cylindrical section.

Figure 4. - Continued. Typical temperature-recovery-factor distribution. Free-stream unit Reynolds number, u_0/ν_0, 6.25×10^5 per inch.

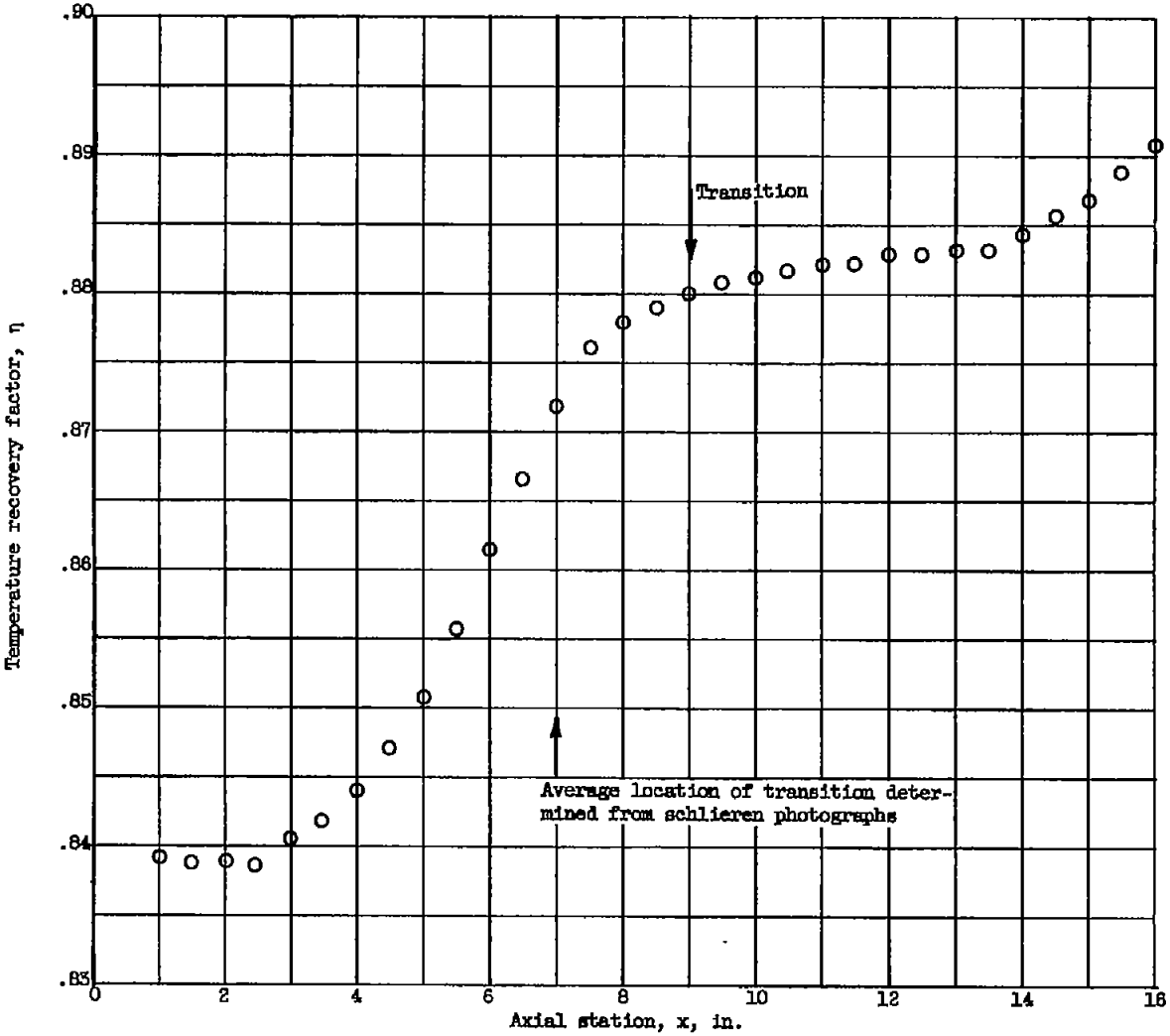

(d) Model 3.

Figure 4. - Continued. Typical temperature-recovery-factor distribution. Free-stream unit Reynolds number, u_0/ν_0, 6.25×10^5 per inch.

4724

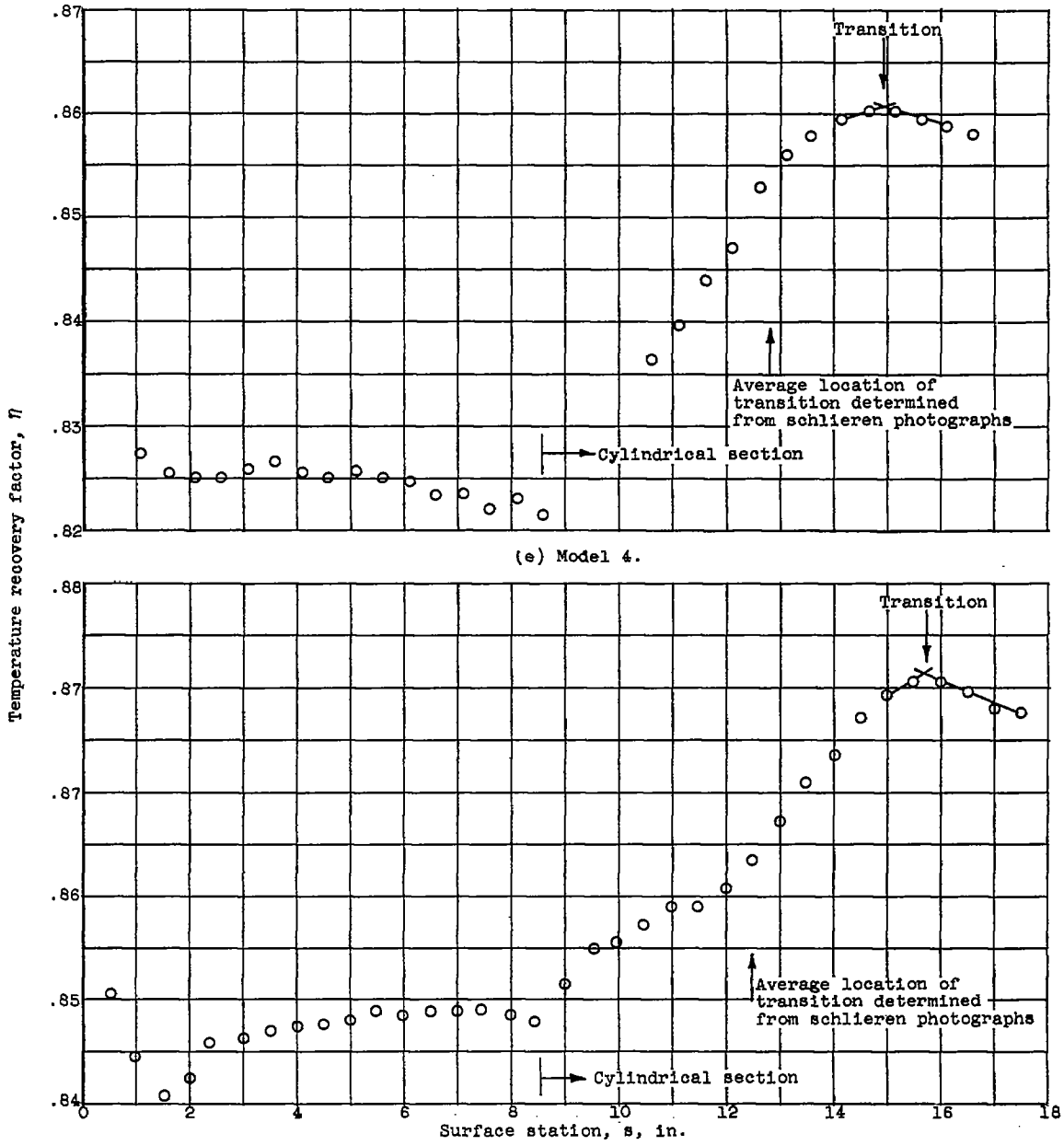

Figure 4. - Concluded. Typical temperature-recovery-factor distribution. Free-stream unit Reynolds number, u_0/ν_0, 6.25×10^5 per inch.

4724

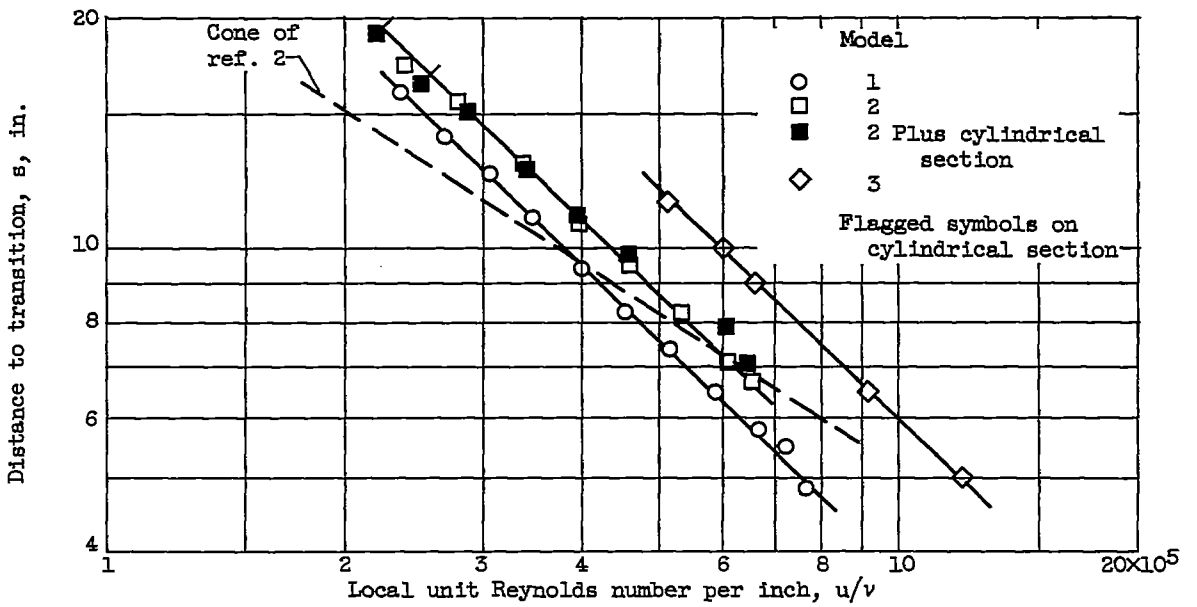

Figure 5. - Effect of unit Reynolds number on location of transition.

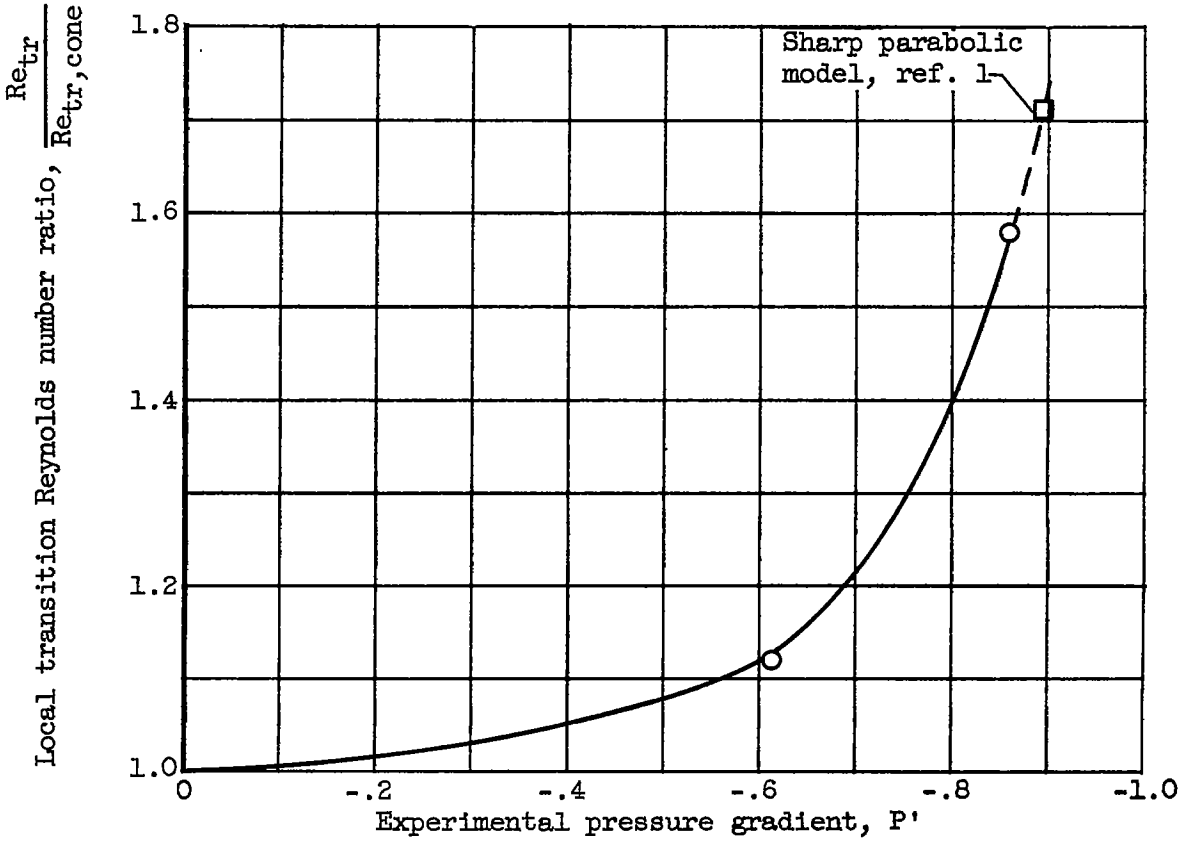

Figure 6. - Effect of pressure gradient on transition Reynolds number.

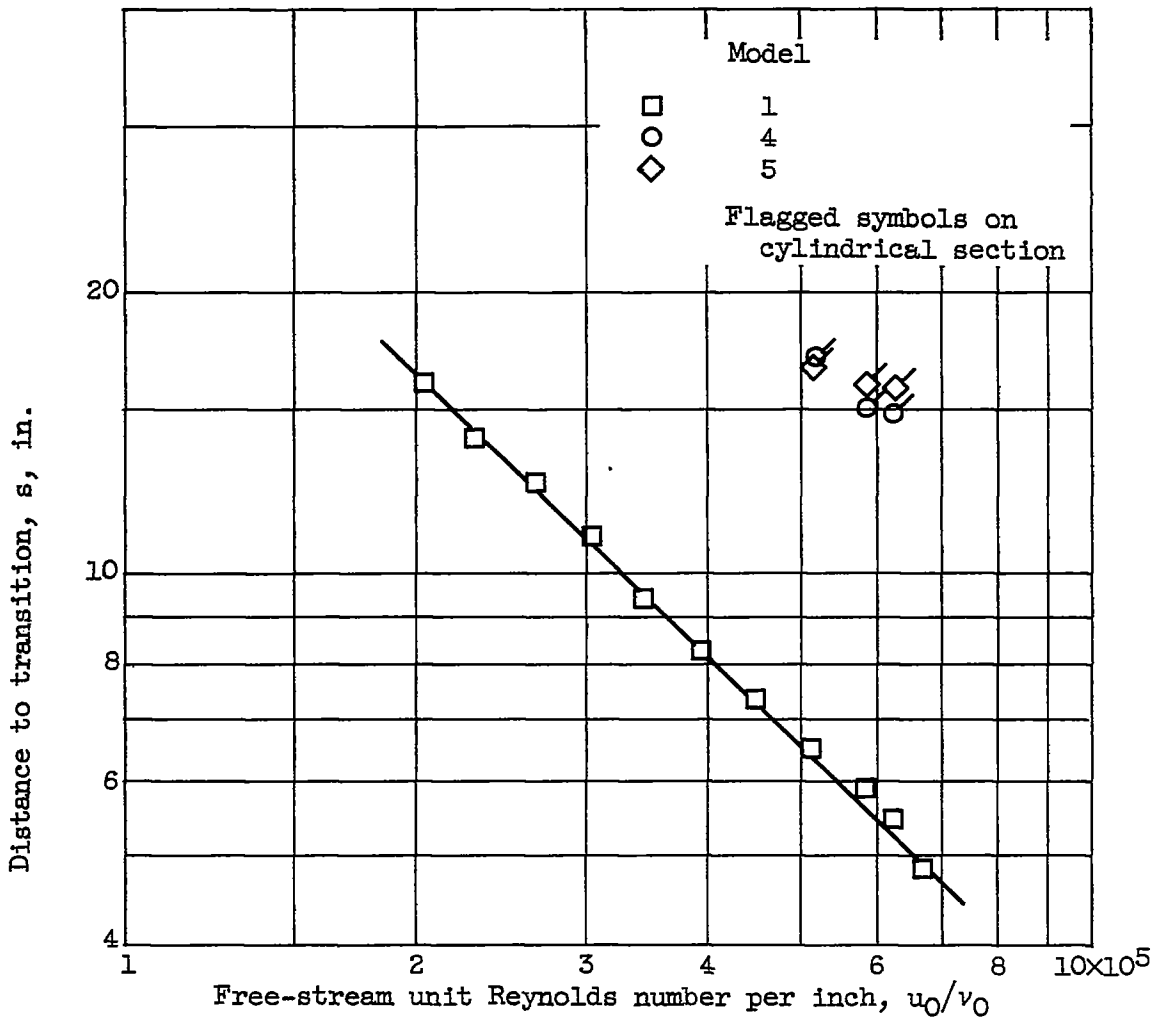

Figure 7. - Combined effect of blunting and favorable pressure distribution on location of transition.

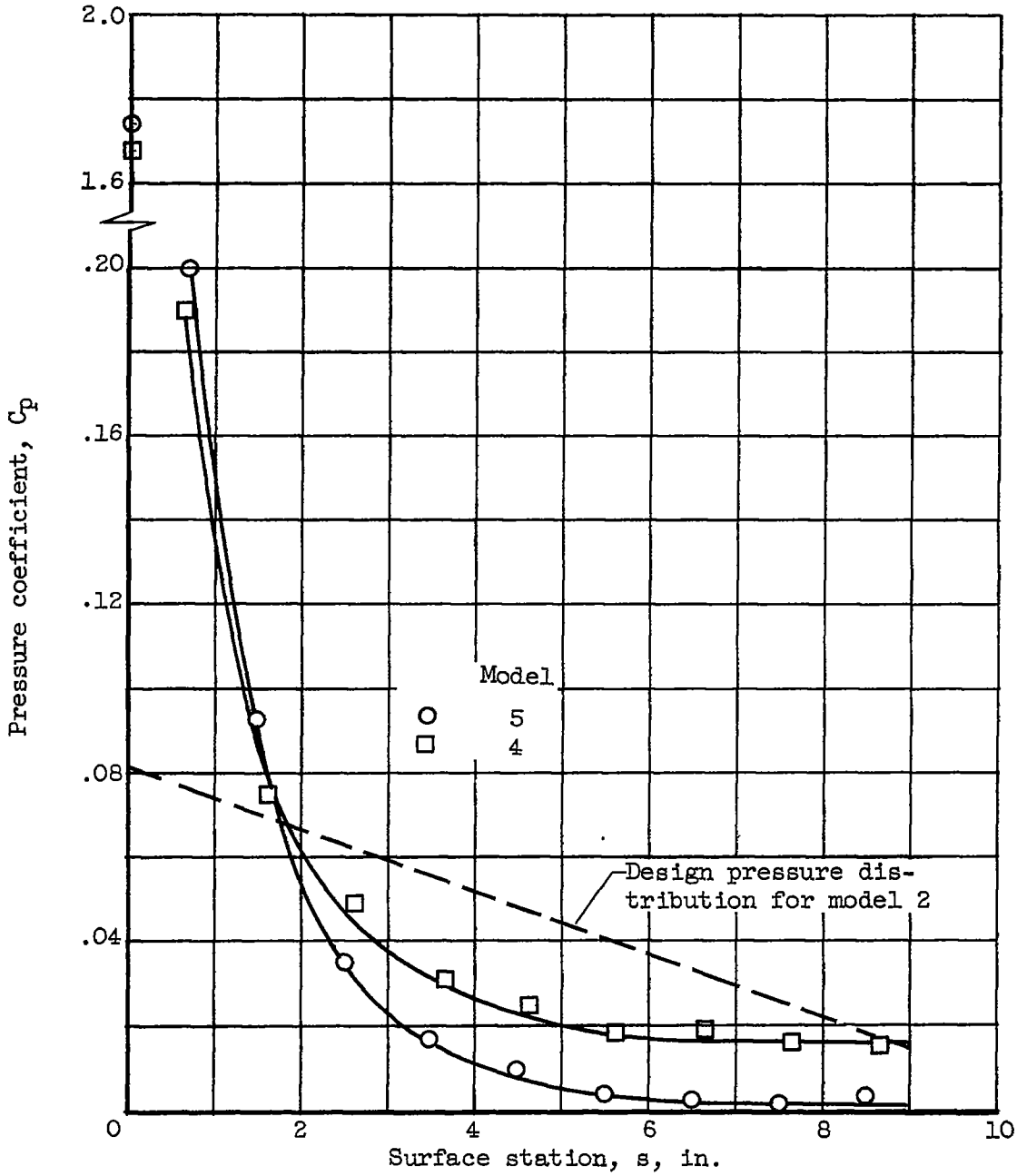

Figure 8. - Forebody pressure distributions.